An efficient method for the creation of tunable optical line traps via control of gradient and scattering forces

Gregory T. Tietjen, Yupeng Kong, and Raghuveer Parthasarathy

Department of Physics and Materials Science Institute, University of Oregon, Eugene, OR 97403-1274

raghu@uoregon.edu

Abstract: Interparticle interaction energies and other useful physical characteristics can be extracted from the statistical properties of the motion of particles confined by an optical line trap. In practice, however, the potential energy landscape, $U(x)$, imposed by the line provides an extra, and in general unknown, influence on particle dynamics. We describe a new class of line traps in which both the optical gradient and scattering forces acting on a trapped particle are designed to be linear functions of the line coordinate and in which their magnitude can be counterbalanced to yield a flat $U(x)$. These traps are formed using approximate solutions to general relations concerning non-conservative optical forces that have been the subject of recent investigations [Y. Roichman, B. Sun, Y. Roichman, J. Amato-Grill, and D. G. Grier, Phys. Rev. Lett. **100**, 013602-4 (2008).]. We implement the lines using holographic optical trapping and measure the forces acting on silica microspheres, demonstrating the tunability of the confining potential energy landscape. Furthermore, we show that our approach efficiently directs available laser power to the trap, in contrast to other methods.

© 2008 Optical Society of America

OCIS codes: (020.7010) Laser Trapping; (170.4520) Optical confinement and manipulation; (230.6120) Spatial light modulators

References and links

1. A. Ashkin, "Optical trapping and manipulation of neutral particles using lasers," Proc. Natl. Acad. Sci. USA **94**, 4853-4860 (1997).
2. D. G. Grier, "A Revolution in Optical Manipulation," Nature **424**, 810-816 (2003).
3. E. M. Furst, "Applications of laser tweezers in complex fluid rheology," Curr. Opin. Colloid Interface Sci. **10**, 79-86 (2005).
4. J. C. Crocker and D. G. Grier, "Microscopic measurement of the pair interaction potential of charge-stabilized colloid," Phys. Rev. Lett. **73**, 352-355 (1994).
5. J. Liphardt, S. Dumont, S. B. Smith, I. Tinoco, Jr., and C. Bustamante, "Equilibrium information from nonequilibrium measurements in an experimental test of Jarzynski's equality," Science **296**, 1832-1835 (2002).
6. K. Svoboda and S. M. Block, "Biological applications of optical forces" Annu. Rev. Biophys. Biomol. Struct. **23**, 247-285 (1994).
7. P. L. Biancaniello, A. J. Kim, and J. C. Crocker, "Colloidal interactions and self-assembly using DNA hybridization," Phys. Rev. Lett. **94**, 058302 (2005).
8. Y. Roichman and D. G. Grier, "Projecting Extended Optical Traps With Shape-Phase Holography," Opt. Lett. **31**, 1675-1677 (2006).
9. T. Yu, F.-C. Cheong, and C.-H. Sow, "The manipulation and assembly of CuO nanorods with line optical tweezers," Nanotechnology **15**, 1732-1736 (2004).
10. R. Verma, J. C. Crocker, T. C. Lubensky, and A. G. Yodh, "Entropic colloidal interactions in concentrated DNA solutions," Phys. Rev. Lett. **81**, 4004-4007 (1998).

#95244 - $15.00 USD Received 22 Apr 2008; revised 19 May 2008; accepted 5 Jun 2008; published 26 Jun 2008

11. Optical forces are, in general, non-conservative (see Ref. [16] and references therein) and so measurements of forces reveal pseudopotentials rather than true potential energy functions. In one dimension, however, any force that depends only on position is necessarily conservative since its integral is uniquely determined. The experiments described here involve only one-dimensional force characterizations, and so determine an effective potential $U(x)$ corresponding to the *x*-axis components of forces; they do not determine the 3D pseudopotential.
12. J. E. Curtis, B. A. Koss, and D. G. Grier, "Dynamic holographic optical tweezers," Opt. Commun. **207**, 169-175 (2002).
13. M. Reicherter, T. Haist, E. U. Wagemann, and H. J. Tiziani, "Optical Particle Trapping With Computer-Generated Holograms Written on a Liquid-Crystal Display," Opt. Lett. **24**, 608-610 (1999).
14. G. Sinclair, P. Jordan, J. Courtial, M. Padgett, J. Cooper, and Z. J. Laczik, "Assembly of 3-Dimensional Structures Using Programmable Holographic Optical Tweezers," Opt. Express **12**, 5475-5480 (2004).
15. A. J. DeWeerd and S. E. Hill, "The Dizzying Depths of the Cylindrical Mirror," The Physics Teacher **43**, 90-92 (2005).
16. Y. Roichman, B. Sun, Y. Roichman, J. Amato-Grill, and D. G. Grier, "Optical Forces Arising from Phase Gradients," Phys. Rev. Lett. **100**, 013602-4 (2008).
17. The CCD pixel intensity was verified to be a linear function of the applied laser power, with a coefficient of determination ("R^2") of 0.9992. The intensity profiles along *x* are measured along the image row of greatest intensity, averaged over adjacent rows spanning $\pm 0.3\mu$m in *y*.
18. J. C. Crocker and D. G. Grier, "Methods of Digital Video Microscopy for Colloidal Studies," J. Coll. Interf. Sci. **179**, 298-310 (1996).
19. S. K. Sainis, V. Germain, and E. R. Dufresne, "Statistics of particle trajectories at short time intervals reveal fN-scale colloidal forces," Phys. Rev. Lett. **99**, 018303 (2007).
20. A total of approximately ten thousand Δx values were recorded for each line. We find no apparent variation of $s_{x_i}^2$ with position or with σ_m; its value yields a diffusion coefficient $D = 0.068 \pm 0.006 \mu\text{m}^2/\text{s}$. In the $F(x)$ plot of Fig. 3(b) (inset), the mean value of F is subtracted; this position-independent force is likely due to convective flow in the chamber or gravitational forces caused by substrate tilt. This offset is irrelevant to the determination of the slope, *B*.
21. The value of *B* for any line trap was determined by a linear fit of all the Δx vs. *x*, to avoid artefacts related to the binning of data. As follows from the discussion in the main text, *B* is equal to the slope of this Δx vs. *x* fit times $2k_BT/s^2$, where s^2 is the position-independent mean of $s_{x_i}^2$.
22. M. Gu, *Advanced Optical Imaging Theory* (Springer, Berlin, 2000).
23. M. F. Hsu, E. R. Dufresne, and D. A. Weitz, "Charge stabilization in nonpolar solvents" Langmuir **21**, 4881-4887 (2005).

1. Introduction

The past few decades have seen remarkable advances in our understanding of interactions between light and matter, one consequence of which has been the development of optical trapping techniques for micromanipulation. It is well known that light focused to a diffraction-limited point attracts dielectric particles; the use of point traps has revolutionized biophysics and the study of soft condensed matter [1, 2, 3, 4, 5, 6]. Several researchers [7, 8, 9, 10] have realized the appeal of *line* traps – 1D trapping potentials – for measuring inter-particle interaction energies and other crucial determinants of material response. In the simplest case, two particles diffusing along a line will sample pair separations, r, whose probability distribution, $p(r)$, obeys a Boltzmann relation, $U(r)/k_BT = -\ln(p(r))$, where U is the interaction energy, k_B is Boltzmann's constant and T is the temperature. There exists, however, a serious obstacle to simply translating passive observations of Brownian motion into measures of interparticle interactions. In order for the dynamics to be determined solely by inter-particle interactions, as the above relation assumes, the line trap's confining potential must be uniform along the line dimension. This condition of uniformity is, in general, *not* true. As we demonstrate and explain below, even light focused to a uniform 1D intensity profile can create a potential landscape that directs particles away from the line center. We have therefore invented a new class of optical line traps that provide tunable intensity profiles along the line, $I(x)$, while conserving the total integrated optical intensity. These profiles are designed to generate forces acting on a trapped particle that vary linearly with the distance from the line center, *x*, and whose slope is an experimentally adjustable parameter. Implementing this approach and measuring $U(x)$ for silica microspheres,

#95244 - $15.00 USD Received 22 Apr 2008; revised 19 May 2008; accepted 5 Jun 2008; published 26 Jun 2008
(C) 2008 OSA

we experimentally demonstrate the construction of one-dimensional trapping potentials (see comment [11]) that are controllably concave up, concave down, or flat.

Our experimental design makes use of holographic optical tweezers (HOT), in which a liquid crystal spatial light modulator (SLM) acts as a programmable diffractive element, modifying the phase of an incident laser wavefront at each pixel [2, 12, 13, 14]. The SLM is located in a plane, P_C, conjugate to the back focal plane of a microscope objective lens. HOTs have recently been exploited to create spatially extended traps by a method very different from ours [8], in which the amplitude profile of the modified laser beam is cleverly mapped onto the SLM phase profile. Using this technique, Roichman et al. have shown that the laser field can be manipulated to control the force landscape experienced by trapped particles [16]; this control, however, comes at the expense of a drastic reduction in diffraction efficiency. In our approach, the intensity profile is reshaped without loss of trap power, allowing micromanipulation over tens of μm length-scales with only tens of milliwatts of total laser power. Our design is constructed from a simple geometric optics perspective that reveals an efficient, approximate solution to the generalized force relations described in Ref. [16].

2. Line trap design and optical forces

Before discussing our design, we first note some elementary properties of optical elements situated at P_C (Fig. 1(a)). A mirror that tilts the incident beam away from the optical axis generates a displaced point trap in the front focal plane, P_F, by imparting to the laser beam a phase profile $\phi(u,v)$ that is linear in u and v, coordinates spanning P_C. The gradient of $\phi(u,v)$ describes the tilt of the reflected beam and therefore the trap displacement, x, in P_F. For a mirror tilted about the v axis by angle θ, $\frac{d\phi}{du} = \frac{2\pi}{\lambda}\theta$, where $\theta \approx x/f$ and f is the focal length of the objective lens. An extended line of uniform intensity in P_F can be created by a continuum of mirrors in P_C, with each increment du equally weighted so that $d\theta/du =$ constant, i.e. $\theta \sim u$. Therefore, $\phi(u) \sim u^2$. Specifiying the endpoints of the line in P_F, e.g. $x = \pm L/2$ for a line of length L, and the extent of the phase profile in P_C, $u = \pm u_{\max}$, fully determines ϕ:

$$\phi(u) = \pi L u^2/(2\lambda f u_{\max}). \tag{1}$$

The phase control at each pixel provided by the SLM enables, in practice, this conceptual decomposition of a phase profile into a set of mirror elements.

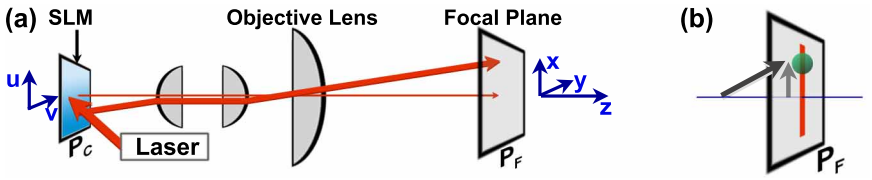

Fig. 1. (a) Simplified schematic of the setup highlighting coordinate axes and focal planes. Thick arrow: a beam deflected from the optical axis (z). Thin arrow: an undeflected beam. For clarity, angles are greatly exaggerated and refraction at the lenses is only approximately indicated. (b) Illustration of the mean radiation force (darker gray arrow) and its nonzero x-component (lighter gray arrow) for a particle located at a position in the line trap (red line) away from the optical axis.

The well known $\phi(u)$ described by Eq. (1) is that of a cylindrical mirror [8, 9]. It possesses an inherent astigmatism which leads, in addition to the desired focal line, to a perpendicular line displaced along the optical axis [8, 15]. This unintended line can be moved "above" or "below" the desired line, i.e. upstream or downstream along the optical axis, by inverting the sign of

#95244 - $15.00 USD Received 22 Apr 2008; revised 19 May 2008; accepted 5 Jun 2008; published 26 Jun 2008
(C) 2008 OSA

ϕ and can therefore be situated outside the experimental sample volume, where it does not interact with particles. In addition to the unintended line, there also exists a more pernicious problem: while this $\phi(u)$ does successfully create a uniform line intensity it does not create a uniform trapping potential for colloidal particles. Rather, as the data below demonstrate, a trapped microparticle is subjected to an outward force that increases linearly with distance from the line center and so is especially significant for lines more than a few μm in extent. This force can be understood from a simple geometric perspective (expanded upon in Section 4) that allows the design and implementation of new types of line traps, as detailed below.

From this point of view we can consider the forces associated with optical trapping as separable into two components: radiative forces, directed along the direction of light propagation and proportional to the intensity, I, and gradient forces, proportional to $\vec{\nabla}I$. In a line trap, the radiative force, F_r, at positions away from the optical axis has a nonzero component along the line direction that grows linearly with x (Fig. 1(b)). The gradient force, F_g, has no component along x for a line of uniform $I(x)$. The sum $F_r + F_g$ creates a concave-down potential which pushes microparticles towards the endpoints of the line, as we experimentally demonstrate below.

To design a uniform trapping potential or, more generally, a potential with some desired, tunable $F(x)$, we need control of F_r and F_g. As noted above, F_r is proportional to x and to I: $F_r \sim xI(x)$. F_g (along the line axis) is given by $F_g \sim dI/dx$. Balancing the two requires:

$$xI(x) - A\frac{dI}{dx} = 0, \tag{2}$$

where A is a constant determined by position-independent optical factors in F_g and F_r (particle size, laser wavelength, index of refraction, etc.). Eq. (2) is satisfied by a Gaussian $I(x)$:

$$I(x) = C\exp\left(-x^2/(2\sigma^2)\right), \tag{3}$$

where C is any constant, provided that $\sigma^2 = A$. If $\sigma^2 > A$, the outward radiative force outweighs the inward gradient force; if $\sigma^2 < A$, the opposite is true .

To create the $\phi(u)$ that generates the above Gaussian $I(x)$, we must "distort" the cylindrical phase profile discussed earlier. Generalizing our mirror-element method, consider each angular increment $d\theta$ as being generated by an element whose weight, du, varies with θ. Since the deflected intensity $I(\theta)d\theta \sim du$ and $\theta \sim \phi' \sim x$, where ϕ' is the gradient of ϕ, $I \sim (du/d\phi') \sim (du/dx)$. Explicitly incorporating $\phi' = \frac{2\pi}{\lambda f}x$ from earlier,

$$\frac{du}{d\phi'} \sim \exp\left(-\left(\frac{\lambda f}{2\pi}\right)^2 \frac{(\phi')^2}{2\sigma^2}\right). \tag{4}$$

Integrating and setting $\phi'_{(u=0)} = 0$ (i.e. defining the central mirror segment as "flat"): $u \sim \left(\pi\sqrt{2\pi}\sigma/(\lambda f)\right)\ \mathrm{erf}\left(\lambda f\phi'/(2\pi\sqrt{2}\sigma)\right)$, where erf is the error function. Incorporating all the prefactors into a constant, D, and defining erfinv as the inverse of the error function:

$$\phi'(u) = \left(2\pi\sqrt{2}\sigma/(\lambda f)\right)\mathrm{erfinv}\,(u/D). \tag{5}$$

The endpoints of the line, set by the values of $\phi'(u = \pm u_{\max})$, occur at $x = \pm L/2$, from which

$$\phi'(u = \pm u_{\max}) = \frac{2\pi}{\lambda f}\left(\pm\frac{L}{2}\right) = \pm\frac{\pi L}{\lambda f}, \tag{6}$$

allowing the determination of D as $D = u_{\max}\left[\mathrm{erf}\left(L/(2\sqrt{2}\sigma)\right)\right]^{-1}$. Thus:

$$\phi'(u) = \left(\frac{2\sqrt{2}\pi}{\lambda f}\sigma\right)\mathrm{erfinv}\left(\frac{u}{u_{\max}}\ \mathrm{erf}\left(\frac{L}{2\sqrt{2}\sigma}\right)\right). \tag{7}$$

#95244 - $15.00 USD Received 22 Apr 2008; revised 19 May 2008; accepted 5 Jun 2008; published 26 Jun 2008
(C) 2008 OSA

Eq. (7) yields a simple cylindrical mirror as $\sigma/L \to \infty$.

3. Experimental characterization of line shapes and trapping forces

Numerically integrating Eq. (7) provides a phase profile, $\phi(u)$, that generates a line trap with a Gaussian intensity profile of width σ (Eq. (3)). Examples of $\phi(u)$ are plotted in Fig. 2(a). Experimentally implementing this, we measure and plot $I(x)$ for a range of σ (Fig. 2). These and other lines are formed using a 655 nm wavelength, 60 mW laser (Meshtel #RS655-70) shaped by a HoloEye 1080P SLM and focused by a NA=1.2 60$\times$ water-immersion lens (Nikon) on a Nikon TE2000-S microscope. For all lines shown, $L = 60\mu$m. Brightfield images are acquired using a CCD camera (Optronics Microfire). Home-made software written in MATLAB calculates ϕ for the SLM and also controls image acquisition. The line is imaged by capturing its reflection at a glass-water interface [17]. We find that the observed intensities are well fit by Gaussian lineshapes (Fig. 2(b)).

The above analysis assumes a uniform intensity profile for the incident beam. A non-uniform profile will lead the measured σ (denoted σ_m) to differ from the intended value (σ_i). For a Gaussian beam of width b (a few mm), one would expect the beam and line profiles to be multiplied to yield a Gaussian product with $\sigma_m^{-2} = cb^{-2} + \sigma_i^{-2}$, where c is a magnification factor. Plotting σ_m^{-2} versus σ_i^{-2} we confirm this linear relation of slope unity (Fig. 2(c)); the measured slope is 0.99 $\pm$ 0.03. The total line intensity (I integrated over x) is found to be nearly constant as a function of σ_m over the measured range $3 < \sigma_m < 17\mu$m (Fig. 2(c), inset); the phase modulation acts to redistribute light, conserving its overall intensity, in stark contrast to other line-shaping approaches [8]. The line width in the transverse (y) direction is measured to be $0.22 \pm 0.01\mu$m for all lines examined, uncorrelated with the Gaussian width in x.

To characterize the optical trapping potentials experienced by colloidal particles, we examined single trapped microspheres of radius $a = 1.6\mu$m silica (Bangs Laboratories) in deionized water (18.2 MΩ-cm, Millipore). These particles are sufficiently dense to gravitationally settle near the chamber bottom, limiting appreciable Brownian motion to the xy plane and allowing characterization of the $x-$component of the trapping force without complications from motion in z [11]. Tracking was performed using home-made software implementing well-established algorithms [18] that localize particle centers with ≈ 20 nm precision. Before presenting quantitative discussions of the trapping landscape, we plot typical trajectories of trapped microparticles that illustrate concave-down, concave-up, and roughly flat potentials. A particle initially at the line center ($x = 0$) experiencing a nearly flat intensity profile ($\sigma_i = \infty$, $\sigma_m = 17.2\mu$m) shows a steady drift away from the line center toward either of the ends (Fig. 3(a), black), *not* free diffusion. For much smaller σ_m, e.g. 3.8μm (Fig. 3(a), dark gray), particle motion is constrained to the vicinity of $x = 0$. The plotted trajectory shows a standard deviation of the position in x of 0.5 μm – considerably smaller than σ_m. For intermediate σ_m, e.g. 8.4μm, the particle meanders with a span of several μm (Fig. 3(a), light gray), suggesting a balance between F_g and F_r. Measurements of trajectories are in themselves insufficient to prove such a balance or to adequately characterize the trapping landscape unless impractically long measurement times are employed. We therefore turn to a more insightful method.

Particle tracking microscopy of Brownian motion can quantify the forces acting on colloidal particles with fN-scale sensitivity (described in detail by Sainis *et al.* [19]). Given an initial position x_i, the statistical ensemble of displacements, Δx_i, over a time increment Δt is described by a diffusive relation $s_{x_i}^2 = 2D_i\Delta t$ and a drift relation $< \Delta x_i >= v_i\Delta t$, where D_i is the diffusion coefficient, v_i is the drift velocity, and $s_{x_i}^2$ and $< \Delta x_i >$ are the variance and mean, respectively, of the measured Δx_i. The force $F_i = bv_i$, where b is the viscous drag, can be evaluated via the Stokes-Einstein relation $D_i = k_BT/b$ to yield $F_i = 2k_BT < \Delta x_i > /s_{x_i}^2$, relating the force at position x_i to the statistics of the displacements without requiring *a priori* knowledge of D.

#95244 - $15.00 USD Received 22 Apr 2008; revised 19 May 2008; accepted 5 Jun 2008; published 26 Jun 2008
(C) 2008 OSA

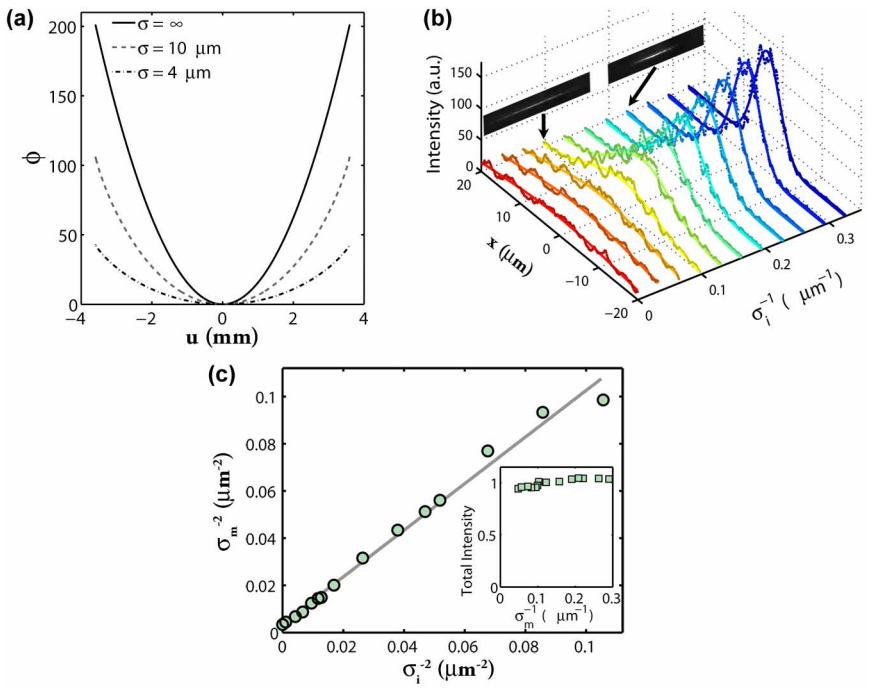

Fig. 2. (a) Phase profiles $\phi(u)$ for various values of σ with parameters $L = 60\mu$m, $f = 2.57$ mm, $\lambda = 0.655\mu$m, and $u_{\max} = 3.6$ mm. (b) Measured intensity profiles, $I(x)$, of Gaussian line traps, together with Gaussian fits. Inset: Images of two of the lines. (c) Measured (σ_m) and intended (σ_i) widths. A linear fit of σ_m^{-2} vs. σ_i^{-2} has slope 0.99 ± 0.3. Inset: Integrated line intensity as a function of σ.

We implemented this method by repeatedly directing a trapped particle to various locations along x, releasing the particle in the line trap, and monitoring the displacements, Δx, over time intervals set by the camera frame rate ($\Delta t = 0.1$ s) [20]. The data reveal a linear relation between F and x, consistent with the earlier discussion (Fig. 3(b), inset). Superimposed on the linear form, $F(x)$ for this and other σ values shows "wiggles" most likely due to the roughness in the intensity profile (Fig. 2(b)), stemming from the pixellation and necessarily imperfect diffraction efficiency inherent in any SLM. We fit $F(x)$ to a linear form and extract the slope, B [21].

The key characterization of the trap potential is the dependence of B on σ. From the above analysis of forces we can interpret σ as a relative weighting of the "inward" F_g and the "outward" F_r. A plot of the measured slope B vs. σ_m^{-1} is shown in Fig. 3(b). For large σ_m, $B > 0$, indicating a net outward force, while for small σ_m, $B < 0$, indicating an inward force. B crosses zero at $\sigma_m = 8.4 \pm 0.7\mu$m – i.e. a Gaussian intensity profile with a width of 8.4 μm leads to a flat trapping potential. (The uncertainty in this critical σ_m is estimated from a linear fit to the $5 < \sigma_m < 17\mu$m data.)

4. Further discussion of optical forces

The simple geometric optics perspective considered in Section 2 is sufficient to describe the data and also provides an intuitive picture of line trap design. This approach can be elaborated upon in light of recent advances in the understanding of non-conservative optical forces relevant for trapping [16]. Roichman *et al.* note that the radiative force can be separated into a component along the optical axis $F_z \sim I$ and components transverse to the optical axis $F_\perp \sim I\ \vec{\nabla}\phi$.

#95244 - $15.00 USD Received 22 Apr 2008; revised 19 May 2008; accepted 5 Jun 2008; published 26 Jun 2008
(C) 2008 OSA

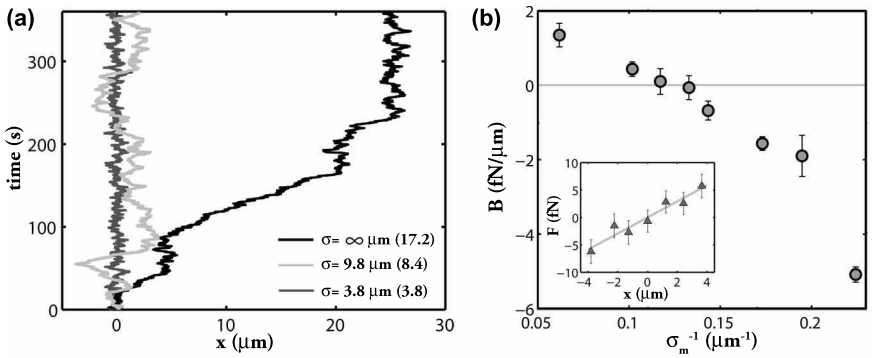

Fig. 3. (a) Representative trajectories of radius $a = 1.6\mu$m silica microspheres initially at the center ($x = 0$) of line traps with intensities $I(x) \propto \exp(-x^2/(2\sigma^2))$. The σ_i values are listed first, with the measured σ_m in parentheses. (b) The dependence of B, the measured slope of F vs. x, on the Gaussian width σ_m. B crosses zero at $\sigma_m = 8.4 \pm 0.7\mu$m, revealing the "flat" line trap for which radiation and gradient forces balance. Inset: The measured position-dependent force, $F(x)$, for $\sigma_i = \infty$.

Phase gradients therefore generate forces in the focal plane, an effect that Roichman *et al.* have exploited to modulate colloidal particle dynamics in both linear and circular geometries [16]. Our expression $F_r \sim xI(x)$ preceding Eq. (2) for the radiative force in the x direction due to an incident ray is therefore equivalent to the phase-gradient formulation if and only if the phase profile is quadratic in the focal plane, P_F, i.e. $\phi(x) \sim x^2$.

The cylindrical mirror phase profile that began our discussion of line traps is quadratic in the SLM plane, P_C, i.e. $\phi(u) \sim u^2$ (see Eq. (1)). The complex electric fields $\tilde{E}(x)$ and $E(u)$ at P_F and P_C, respectively, are related by Fourier transformation [22]:

$$\tilde{E}(x) = \frac{1}{f\lambda} \int E(u) \exp\left(j \frac{2\pi}{f\lambda} xu\right) du. \tag{8}$$

The SLM modulates the phase and not the amplitude of the optical field, and so $E(u) = E_0 \exp(j\phi(u))$, where E_0 is a constant and $\phi(u)$ is given by Eq. (1). Applying Eq. (8), $\tilde{E}(x) = \tilde{E}_0 (f\lambda)^{-1} \exp(j\phi(x))$ with

$$\phi(x) = \frac{2\pi u_{\max}}{f\lambda L} x^2. \tag{9}$$

In other words, a quadratic phase profile in P_C creates a quadratic phase profile in P_F and therefore a geometric factor in F_r that increases linearly with x.

The phase profiles of our Gaussian traps (Eq. (7)) are not simple quadratic functions and are not amenable to analytic Fourier transformation. Plots of $\phi(u)$ (Fig. 2(a)) show, however, that the deviations from parabolic shapes are small enough that $\phi(u)$ can be approximated by a series expansion in u^2 up to second order. The $\phi(u)$ obtained from Eq. (7) differ from the form $\phi(u) = au^2 + bu^4$ by a root-mean-square deviation of less than 0.5 radians and yield a mean value of bu^4/au^2 less than 0.12 over the full range of σ_i examined. Applying Eq. (8) to $E(u) = E_0 \exp(j\phi(u))$ with phase factor $\phi(u) = au^2 + bu^4$ and keeping only the lowest order terms in bu^2/a, $\tilde{E}(x) = \tilde{E}_0 (f\lambda)^{-1} \exp(j\phi(x))$ with

$$\phi(x) = \frac{2\pi u_{\max}}{f\lambda L} x^2 \left[1 - \frac{4b}{a^3}\left(\frac{\pi}{f\lambda}\right)^2 x^2\right], \tag{10}$$

#95244 - $15.00 USD Received 22 Apr 2008; revised 19 May 2008; accepted 5 Jun 2008; published 26 Jun 2008
(C) 2008 OSA

where the second term in brackets is small compared to 1. Therefore the $\phi(u)$ of our Gaussian lines lead to phase profiles $\phi(x)$ in the focal plane that are similar enough to parabolic forms to make $F_r \sim xI(x)$ a reasonable approximation to the true transverse radiative force.

This analysis raises the question: why not generate a field distribution in P_F with an *exactly* quadratic $\phi(x)$ and a Gaussian intensity profile? Such a field can provide balanced forces, as seen by the generalized form of Eq. (2),

$$\frac{d\phi}{dx}I(x) - A\frac{dI}{dx} = 0. \tag{11}$$

Similarly, a line trap with constant $\phi(x)$ and $I(x)$ will also provide zero net force on trapped particles. In both of these cases, and in general, there is a significant problem with this approach: the desired fields in P_F generate, by Fourier transformation, fields in P_C that vary in *amplitude* as well as *phase*. (In the first case considered above the amplitude will be a Gaussian function of u, in the second a sinc function.) The fields in P_C are implemented by an SLM that modulates only the phase of the incident light; even if it were also to modulate amplitude, such modulation would be undesirable as it would necessarily involve a decrease in optical intensity. Grier and co-workers have invented a method, termed shape-phase holography, by which amplitude modulation can be implemented with a "phase-only" SLM, mapping amplitude variations in $E(u)$ onto the *number* of pixels in v (the orthogonal axis in P_C) that contribute to the line in P_F [8]. Implementing the phase-gradient analysis described above, they have controlled the landscape of forces acting on trapped colloidal particles using constant $I(x)$ and variable $\phi(x)$ [16]. While elegant and effective, the cost in laser power is enormous. For typical line geometries of the sort implemented in our experiments, mapping the amplitude of a sinc function onto the v axis in P_C, for example, leads to less than 10 % of the SLM area contributing to the line trap; over 90 % of the available laser power does not contribute and is wasted.

Therefore, though inexact, our simple method of tuning optical forces in line traps has two important attributes. First, the ray-optics picture provides a framework for the intuitive understanding of trap design. Second, our design efficiently directs available laser power to the line trap, enabling the trapping of micron-scale particles in extended geometries with only tens of milliwatts of total power, due to its intrinsically "phase-only" modulation in the SLM plane. This leads to modulation in the focal plane of *both* $I(x)$ and $\phi(x)$.

5. Conclusions

The potential energy landscape experienced by a line-trapped colloidal particle is a non-trivial function of the line structure. By considering simple yet effective approximations to the optical forces involved, we have designed a family of Gaussian line traps that enables the tuning of that landscape without loss of optical intensity. The width of the Gaussian intensity function is the crucial determinant of the confining potential; the line length, L, defines the extent of the landscape, but σ_m controls its shape. The insights described above should be widely beneficial to the study of colloidal interactions, especially in the case of long-range forces [23]. The optical principles involved are moreover sufficiently general to also apply to very different physical systems, e.g. trapped cold atoms and atomic condensates.

Acknowledgments

We thank Jennifer Curtis, Eric Dufresne, Nancy Forde, Martin Forstner, David Grier, Astrid van der Horst, and Heiner Linke for useful comments and discussions. This work was supported by the Alfred P. Sloan Foundation and the National Science Foundation (Award Number 0746038).

#95244 - $15.00 USD Received 22 Apr 2008; revised 19 May 2008; accepted 5 Jun 2008; published 26 Jun 2008
(C) 2008 OSA